Reactivity of Five-Coordinate Models for the Thiolate-Ligated Fe Site of Nitrile Hydratase

Jeffrey J. Ellison, Andrew Nienstedt, Steven C. Shoner, David Barnhart, Jerry A. Cowen,† and Julie A. Kovacs*

Contribution from the Department of Chemistry, University of Washington, Seattle, Washington 98195

Received September 4, 1997

Abstract: To examine inhibitor binding to an iron site resembling that of the metalloenzyme nitrile hydratase (NHase), a coordinatively unsaturated, five-coordinate Fe^{III} thiolate complex was synthesized, and its reactivity examined. Ferricinium hexafluorophosphate induced oxidation of *gem*-dimethyl-protected $[Fe^{II}S_2{}^{Me2}N_3(Pr,Pr)]$ affords the chiral, five-coordinate complex $[Fe^{III}S_2{}^{Me2}N_3(Pr,Pr)]^+$ (**2**) in reasonable yields. The magnetic properties and EPR of **2** are consistent with an $S = {}^1/_2$ ground state. This unusual spin state, in conjunction with the low coordination number, of **2** result in unusually short Fe−S bonds (2.15(2) Å). Ligand constraints distort the S−Fe−N angles in **2** and create an open (132.3(1)°) reactive site. Azide binds to this site to afford a model for the azide-inhibited form of NHase $[Fe^{III}S_2{}^{Me2}N_3(Pr,Pr)(N_3)]$ (**3**). In MeOH azide binds reversibly, whereas in MeCN it binds irreversibly. This demonstrates that the secondary coordination sphere (i.e., the solvent, or possibly a protein binding pocket) can have a dramatic influence on the substrate binding properties of a metal complex. A variable-temperature equilibrium study in MeOH afforded thermodynamic parameters ($\Delta H = -5.2 \pm 0.9$ kcal/mol and $\Delta S = -12.4 \pm 0.4$ eu) for the binding of this inhibitor. The electronic spectrum of **3** displays an intense band at 708 (1600) nm similar to that (710 (∼1200) nm) of the pH = 7.3 form of NHase, and other six-coordinate *cis*-dithiolate ligated Fe^{III} complexes synthesized by our group. EPR parameters for **3** ($g = 2.23, 2.16, 1.99$) are nearly identical to those of the azide-inhibited form of NHase ($g = 2.23, 2.14, 1.99$), suggesting that (1) the iron site of our model closely resembles that of the enzyme, and (2) azide binds directly to the metal ion in NHase. Reactivity is oxidation-state dependent, and the reduced analogue of **2**, $[Fe^{II}S_2N_3(Pr,Pr)]$ (**4**), reversibly binds CO, but not azide, whereas oxidized **2** binds azide, but not CO.

Introduction

Nitrile hydratase (NHase) is a metalloenzyme which catalyzes the hydrolysis of nitriles to amides.[1−15] It is found in microorganisms such as *Rhodococcus* sp. R312 and N771, and *Pseudomona chlorophis*, and falls into a rare class[16,17] of cysteine-ligated, non-heme iron enzymes. Potential uses for this biocatalyst include the inexpensive production of amides,[18] enantioselective amide synthesis,[10] and conversion of nitrile wastes to less toxic amides.[19] In Japan, microbial NHase is currently being used in the kiloton production of acrylamide.[18] In contrast to most hydrolytic enzymes, NHase has been shown to contain iron, or, in some cases, cobalt,[20,21] as opposed to zinc.[22] Iron-containing *Rhodococcus* sp. R312 and N771 have been most extensively studied. On the basis of EPR,[4] EXAFS,[5,12] and ENDOR studies,[9,23] the NHase active site in these

† Department of Physics, Michigan State University, East Lansing, MI 48824.

(1) Brennan, B. A.; Cummings, J. G.; Chase, D. B.; Turner, I. M., Jr.; Nelson, M. J. *Biochemistry* **1996**, *35*, 10068−10077.
(2) Odaka, M.; Fujii, K.; Hoshino, M.; Noguchi, T.; Tsujimura, M.; Nagashima, S.; Yohada, N.; Nagamune, T.; Inoue, I.; Endo, I. *J. Am. Chem. Soc.* **1997**, *119*, 3785−3791.
(3) Nagasawa, T.; Ryuno, K.; Yamada, H. *Biochem. Biophys. Res. Commun.* **1986**, *139*, 1305−12.
(4) Sugiura, Y.; Kuwahara, J.; Nagasawa, T.; Yamada, H. *J. Am. Chem. Soc.* **1987**, *109*, 5848−50.
(5) Scarrow, R. C.; Brennan, B. A.; Nelson, M. J. *Biochemistry* **1996**, *35*, 10078−10088.
(6) Tsujimura, M.; Odaka, M.; Nagashima, S.; Yohda, M.; Endo, I. *J. Biochem.* **1996**, *119*, 407−413.
(7) Brennan, B. A.; Jin, H.; Chase, D. B.; Turner, I. M.; Buck, C.; Scarrow, R. C.; Gurbiel, R.; Doan, P.; Hoffman, B. M.; Nelson, M. J. *J. Inorg. Biochem.* **1993**, *51*, 373.
(8) Honda, J.; Kandori, H.; Okada, T.; Nagamune, T.; Shichida, Y.; Sasabe, H.; Endo, I. *Biochemistry* **1994**, *33*, 3577−3583.
(9) Jin, H.; Turner, I. M., Jr.; Nelson, M. J.; Gurbiel, R. J.; Doan, P. E.; Hoffman, B. M. *J. Am. Chem. Soc.* **1993**, *115*, 5290−1.
(10) Maddrell, S. J.; Turner, N. J.; Crosby, J. *Tetrahedron Lett.* **1996**, 6001.
(11) Nagamune, T.; Honda, J.; Kobayashi, Y.; Sasabe, H.; Endo, I.; Ambe, F. *Hyperfine Interact.* **1992**, *71*, 1271−1274.
(12) Nelson, M. J.; Jin, H.; Turner, I. M., Jr.; Grove, G.; Scarrow, R. C.; Brennan, B. A.; Que, L., Jr. *J. Am. Chem. Soc.* **1991**, *113*, 7072−3.
(13) Noguchi, T.; Honda, J.; Nagamune, T.; Sasabe, H.; Inoue, Y.; Endo, I. *FEBS Lett.* **1995**, *358*, 9−12.
(14) Noguchi, T.; Hoshino, M.; Tsujimura, M.; Odaka, M.; Inoue, Y.; Endo, I. *Biochemistry* **1996**, *35*, 16777−16781.
(15) Odaka, M.; Noguchi, T.; Nagashima, S.; Yohda, M.; Yabuki, S.; Hoshino, M.; Inoue, Y.; Endo, I. *Biochem. Biophys. Res. Commun.* **1996**, *221*, 146−150.
(16) Tavares, P.; Ravi, N.; Moura, J. J. G.; LeGall, J.; Huang, Y.-H.; Crouse, B. R.; Johnson, M. K.; Huynh, B. H.; Moura, I. *J. Biol. Chem.* **1994**, *269*, 10504−10510.
(17) Chen, L.; Sharma, P.; LeGall, J.; Mariano, A. M.; Teixeira, M.; Xavier, A. V. *Eur. J. Biochem.* **1994**, *226*, 613−618.
(18) Kobayashi, M.; Nagasawa, T.; Yamada, H. *Tibtech* **1992**, *10*, 402−408.
(19) Wyatt, J. M.; Knowles, C. J. *Int. Biodeterior. Biodegrad.* **1995**, *35*, 227−248.
(20) Brennan, B. A.; Alms, G.; Nelson, M. J.; Durney, L. T.; Scarrow, R. C. *J. Am. Chem. Soc.* **1996**, *118*, 9194.
(21) Nagasawa, T.; Takeuchi, K.; Yamada, H. *Eur. J. Biochem.* **1991**, *196*, 581−589.
(22) Eklund, H.; Branden, C.-I. *Zinc Enzymes*; Wiley: New York, 1983.
(23) Doan, P.; Nelson, M. J.; Jin., H.; Hoffman, B. M. *J. Am. Chem. Soc.* **1996**, *118*, 7014−7015.

S0002-7863(97)03129-6 CCC: $15.00
Published on Web 06/02/1998

Table 1. EPR Parameters for Model Compounds vs Non-Heme and Heme Enzymes Nitrile Hydratase (NHase) and Cytochrome P-450

	g values		
$[Fe^{III}S_2{}^{Me2}N_3(Pr,Pr)]^+$ (**2**)2[a]	2.20,	2.15,	2.00
$[Fe^{III}S_2{}^{Me2}N_3(Pr,Pr)(N_3)]$ (**3**)[a]	2.23,	2.16,	1.99
NHase enzyme + N_3^- [b]	2.23,	2.14,	1.99
$[Fe^{III}(ADIT)_2]^+$ (**1**)[c]	2.19,	2.13,	2.01
$[Fe^{III}(AMIT)_2]^+$ (**5**)[c]	2.20,	2.16,	2.00
NHase enzyme (pH = 9)[d,e]	2.20,	2.12,	1.99
NHase enzyme (pH = 7.3)[d,e]	2.27,	2.14,	1.97
NHase enzyme + $(CH_3)_2CHCN$ (pH = 7.2)[b]	2.21,	2.12,	1.98
NHase enzyme + NO[h]	EPR silent		
cytochrome P-450 (oxidized, ls)[f]	2.45,	2.26,	1.91
$[Fe^{III}$(por)(N-MeIm)(S−C_6H_4−*p*-NO_2)$]$[g]	2.42	2.26	1.91

[a] This work. [b] Sugiura, Y.; Kuwahara, J.; Nagasawa, T.; Yamada, H. *J. Am. Chem. Soc.* **1987**, *109*, 5848. [c] Shoner, S. C.; Barnhart, D.; Kovacs, J. A. *Inorg. Chem.* **1995**, *34*, 4517−18. [d] These spectra were recorded in the presence of a butyrate buffer, which was added in order to stabilize the samples. Since butyrate appears to act as an inhibitor[e] the reported *g* values are those a "butyrate-inhibited" form of the enzyme. [e] Brennan, B. A.; Cummings, J. G.; Chase, D. B.; Turner, I. M., Jr.; Nelson, M. J. *Biochemistry* **1996**, *35*, 10068. [f] Tsai, R.; Yu, C. A.; Gunsalus, I. C.; Peisach, J.; Blumberg, W.; Orme-Johnson, W. H.; Beinert, H. *Proc. Natl. Acad. Sci.* **1970**, *66*, 1157−1163. [g] Tang, S. C.; Koch, S.; Papaefthymiou, G. C.; Foner, S.; Frankel, R. B.; Ibers, J. A.; Holm, R. H. *J. Am. Chem. Soc.* **1976**, *98*, 2414−2434. por = protoporphyrin IX dimethyl ester. [h] Nagmune, T.; Honda, J.; Kobayashi, Y.; Sasabe, H.; Endo, I.; Ambe, F. *Hyperfine Interact.* **1992**, *71*, 1271−1274.

bacterial sources has been proposed to contain a six-coordinate, low-spin ($S = {}^1/_2$) Fe^{3+} ion ligated by at least two *cis*-cysteinates, three nitrogens, and a hydroxide:[23]

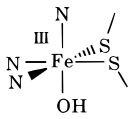

Results from a recent X-ray crystal structure[24] indicate that two amide-type nitrogens, provided by the peptide backbone, and possibly a third conserved[3,25] cysteinate, are coordinated to the metal. The third Fe−S^{cys} bond appears to be significantly longer (∼2.5 Å) than the other two. In fact, given the low resolution (2.65 Å) of this structure[24] it is not clear whether this third sulfur is bound to the iron. If it is not ligated, then it is possible that it plays a role in the mechanism similar to that of the catalytic cysteinate found in nitrilase[26,27]—an enzyme which lacks a metal ion.

The low spin state of the NHase iron site is highly unusual, especially given that π donors (i.e., sulfurs) are present in the coordination sphere. The EPR signal associated with NHase (Table 1) is characteristic of an $S = {}^1/_2$ system containing an odd electron in a d_{xy} orbital.[1] The unusually small g_{max} value (<2.3) suggests that unpaired spin density is delocalized onto some of the ligating atoms. The electronic spectrum of NHase (Table 2; Figure 5) displays a characteristic sulfur-to-iron charge-transfer band near 700 nm which is responsible for the enzyme's green color.[1−4] Both the EPR (Table 1) and electronic spectral (Table 2) properties of NHase are pH-dependent.[1−5] Activity is also pH-dependent; the pH = 9 form is inactive,

Table 2. Comparison of Electronic Spectral Data for Nitrile Hydratase Enzyme vs Five- and Six-Coordinate Model Compounds

	λ_{max} (ϵ)		
$[Fe^{II}S_2N_3(Pr,Pr)]$ (**4**)[a,b]	359 (820)		
$[Fe^{III}S_2{}^{Me2}N_3(Pr,Pr)]^+$ (**2**)[c,d]	416 (4200),	474 (sh)[e]	
$[Fe^{III}S_2{}^{Me2}N_3(Pr,Pr)(N_3)]$ (**3**)[d,f]	330 (7400),	460 (2200),	708 (1600)
$[Fe^{III}(ADIT)_2]^+$ (**1**)[g,h]		438 (3400),	718 (3750)
$[Fe^{III}(AMIT)_2]^+$ (**5**)[g,h]		425 (sh),	696 (2800)
inactive enzyme (pH = 9)[i,j]			690 (∼1200)
active enzyme (pH = 7.3)[i,j]			710 (∼1200)
active enzyme (butyrate-free)[k]			676 (NR)[l]
enzyme + CH_3CH_2CN[m]			690 (∼4200)
NO-inactivated enzyme[n]		370 (∼4300)	

[a] Spectrum recorded in H_2O at ambient temperature. [b] Shoner, S. C.; Nienstedt, A.; Ellison, J. J.; Kung, I.; Barnhart, D.; and Kovacs, J. A. *Inorg. Chem.* **1997**, submitted. [c] Spectrum recorded in MeOH at ambient temperature. [d] This work. [e] Five-coordinate **2** also displays a weaker transition at 774 (440) nm. Only the charge-transfer bands ($\epsilon \geq 800\ M^{-1}\ cm^{-1}$), which dominate the spectra, and which are observable with the native enzyme, are shown. [f] Spectrum recorded in MeOH at −77 °C. [g] Spectrum recorded in MeCN at ambient temperature. [h] Shoner, S. C.; Barnhart, D.; Kovacs, J. A. *Inorg. Chem.* **1995**, *34*, 4517. [i] These spectra were recorded in the presence of a butyrate buffer. [j] Brennan, B. A.; Cummings, J. G.; Chase, D. B.; Turner, I. M., Jr.; Nelson, M. J. *Biochemistry* **1996**, 10068. [k] Honda, J.; Kandori, H.; Okada, T.; Nagamune, T.; Shichida, Y.; Sasabe, H.; Endo, I. *Biochemistry* **1994**, *33*, 3577−3583. [l] NR = not reported. [m] Sugiura, Y.; Kuwahara, J.; Nagasawa, T.; Yamada, H. *J. Am. Chem. Soc.* **1987**, *109*, 5848−50. [n] Odaka, M.; Fujii, K.; Hoshino, M.; Noguchi, T.; Tsujimura, M.; Nagashima, S.; Yohada, N.; Nagamune, T.; Inoue, I.; Endo, I. *J. Am. Chem. Soc.* **1997**, *119*, 3785−3791.

whereas the pH = 7.3 form is active.[7] Substrates (RCN), inhibitors (N_3^-, butyrate), and inactivators (NO),[2,28,29] also have a noticeable affect on both the electronic spectral (Table 2) and EPR (Table 1) properties of the enzyme,[2,4,8,11] possibly suggesting that these bind to the metal ion:

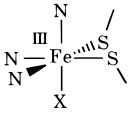

X= RCN, N_3^-, NO, $CH_3(CH_2)_2CO_2^-$

Definitive evidence for this is, however, lacking. Although the mechanism by which nitrile hydratase catalyzes nitrile hydrolysis has not been elucidated, one possibility is that the nitrile substrate displaces the iron-bound hydroxide (once it has been protonated), and is then activated by binding to the Lewis acidic Fe^{3+} ion. The response of the enzyme's EPR signal to added substrate (Table 1) appears to support this mechanism. Also, the large rate enhancement (10^6−10^8) of nitrile hydrolysis observed with synthetic systems containing metal-bound (M^{+3} = Co, Ru, Rh) nitriles, seems to argue in favor of a metal-promoted nitrile activation mechanism.[30−32] Azide-induced inhibition may be caused by its ligation to and blockage of the metal site to which nitriles bind.[1,4]

(24) Huang, W.; Jia, J.; Cummings, J.; Nelson, M.; Schneider, G.; Lindqvist, Y. *Structure* **1997**, 5, 691−699.
(25) Mayoux, J. -.; Cerbeoud, E.; Soubrier, F.; Faucher, D.; Petre, D. *J. Bacteriol.* **1990**, *172*, 6764−6773.
(26) Stevenson, D. E.; Feng, R.; Dumas, F.; Groleau, D.; Mihoc, A.; Storer, A. C. *Biotechnol. Appl. Biochem. Biotechnol.* **1992**, *15*, 283−302.
(27) Dufour, E.; Storer, A. C.; Menard, R. *Biochemistry* **1995**, *34*, 16382−16388.
(28) Scarrow, R. C.; Strickler, B.; Ellison, J. J.; Shoner, S. C.; Kovacs, J. A.; Cummings, J. G.; Nelson, M. J. Manuscript submitted.
(29) Popescue, V.-C.; Munck, E.; Krebs, C.; Pereira, A. S.; Tavares, P.; Huynh, B. H.; Schweitzer, D.; Ellison, J. J.; Kovacs, J. A.; Cummings, J. G.; Turner, I. M., Jr.; Nelson, M. A. Manuscript in preparation.
(30) Zanella, A. W.; Ford, P. C. *Inorg. Chem.* **1975**, *14*, 42−47.
(31) Kim, J. H.; Britten, J.; Chin, J. *J. Am. Chem. Soc.* **1993**, *115*, 3618−3622.
(32) Chin, J. *Acc. Chem. Res.* **1991**, *24*, 145−152.

Synthetic modeling studies should prove useful in the interpretation of nitrile hydratase's spectroscopic responses to added substrate (RCN), inhibitors (azide, butyrate), and inactivators (NO), and should also aid in the elucidation of the mechanism of nitrile hydrolysis, as well as clear up existing uncertainties concerning the number of ligated cysteinates. Ultimately one would hope to determine whether there is any correlation between the iron site structure, resulting biophysical properties, and reactivity. There are, however, challenges to modeling this site. First, the combination of Fe^{III} and thiolates is thermodynamically unstable with respect to Fe^{II} and disulfide formation.[33,34] For this reason, only a small number of Fe^{III} thiolates have been reported, and even fewer have been structurally characterized.[34−42] There are only a handful of mixed N/S-ligated Fe^{III} complexes.[36,39−41,43] Second, low spin-states are unusual for non-heme iron; it is most common for Fe^{III} to be high-spin ($S = {}^5/_2$),[44,45] or, at best, exist as a thermal mixture of low and high spin states ($S = {}^1/_2 \leftrightarrow S = {}^5/_2$), when in a classical coordination environment.[39,41,46] The ability of sulfur to form highly covalent bonds, however, may reduce the pairing energy (the nephelauxetic effect)[47] and thereby stabilize a low-spin state. Third, Fe thiolate complexes tend to possess labile metal−ligand bonds. This interferes with the isolation, and reactivity studies, of synthetic models. To synthesize a well-defined active site model, for which lability is decreased, one commonly utilizes multidentate ligands. In most cases these are not commercially available, so that ligand design and synthesis plays a significant role in modeling. Using a "one-pot" synthesis, involving a metal-templated Schiff base condensation, we can access a variety of mixed N/S-ligated metal complex structures, that appear to be robust, yet reactive, and capable of stabilizing Fe^{III} thiolates, in a $S = {}^1/_2$ spin state.[43,48−50] We have shown that linear multidentate ligands, composed of ethyl- or propylamine chains, imine linkages, and terminal thiolate sulfurs, allow enough flexibility in metal−ligand interaction to accommodate a variety of metal ions, in multiple oxidation states.[48−51]

In a previous paper we described a synthetic analogue of nitrile hydratase, $[Fe^{III}(ADIT)_2]Cl$ (**1**),[43] which is remarkably similar to the enzyme active site in terms of its electronic and geometric structure. For example, the crystallographically

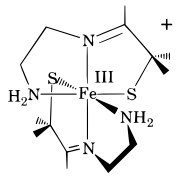

$[Fe^{III}(ADIT)_2]^+$ (**1**)

determined mean Fe−S distance (2.205(5)) Å in **1** is virtually identical to the EXAFS-determined Fe−S distance (2.21(3) Å) of the enzyme. These short distances distinguish **1** from most other iron thiolates,[34−43] and reflect the highly unusual low-spin state of this site.[43] The magnetic properties of **1** indicate that it possesses an $S = {}^1/_2$ ground state over the temperature range 10−400 K. This spin-state assignment is confirmed by EPR at 77 K (Table 1). The electronic spectrum of **1** is virtually identical to that of the enzyme, and contains a sulfur-to-metal charge-transfer band near 700 nm (Table 2) that appears to be diagnostic of six-coordinate thiolate-ligated structures of this type, and highly sensitive to the local Fe environment.[51] This close match in properties suggests that our model contains iron in a site which closely resembles that of NHase.

Reactivity is a more challenging aspect of metalloenzyme chemistry to model. It requires that the metal ion be in either a coordinatively unsaturated environment, or one which is asymmetric with one labile site. This is especially challenging when thiolates are contained in the coordination sphere, since they tend to form bridges,[52,53] which encourage either polymer or cluster formation, making the labile or vacant site inaccessible. Herein, we report the synthesis, structure, and reactivity of a five-coordinate Fe^{III} bis(thiolate) complex, which reversibly binds the enzyme inhibitor N_3^- to form a model for the azide-inhibited form of nitrile hydratase.

Experimental Section

General Methods. Unless noted otherwise, all reactions were carried out under nitrogen at room temperature using Schlenk-line or drybox techniques. Solvents were dried over calcium hydride (MeCN), sodium benzophenone (Et_2O), and magnesium turnings (MeOH, EtOH) and freshly distilled under nitrogen and degassed prior to use. Ferrocenium hexafluorophosphate[54] was synthesized as described in the literature. Anhydrous ferrous chloride (Strem), tetrakis *n*-butylammonium azide (TCI), and *N*-(3-aminopropyl)-1,3-propanediamine (Aldrich) were purchased commercially and used as received. NMR spectra were recorded on a Bruker AC-200, AF-300, or VXR-500 spectrometer. IR samples were prepared as either KBr pellets (solid state), or MeOH, or CH_2Cl_2 solutions in matched cells, and IR spectra were obtained using a Perkin-Elmer 1600 FTIR. A Hewlett-Packard Model 8450 spectrometer, interfaced to an IBM PC was used to record UV/vis/near-IR spectra. Solution magnetic moments were determined using the Evans' method, as corrected for superconducting solenoids.[55] Magnetic susceptibility measurements in the solid state were done using a Quantum Design MPMS SQUID susceptometer at Michigan State University. Elemental analyses were performed by Galbraith Labs, Knoxville, TN. EPR spectra were recorded on an EPX Bruker. Cyclic

(33) Herskovitz, T.; Depamphilis, B. V.; Gillum, W. O.; Holm. R. H. *Inorg. Chem.* **1975**, *14*, 1426−30.
(34) Millar, M.; Lee, J. F.; Fikar, R. *Inorg. Chim. Acta* **1996**, *243*, 333.
(35) Maelia, L. E.; Millar, M.; Koch, S. A. *Inorg. Chem.* **1992**, *31*, 4594−600.
(36) Govindaswamy, N.; Quarless, D. A., Jr.; Koch, S. A. *J. Am. Chem. Soc.* **1995**, *117*, 8468−69.
(37) Lane, R. W.; Ibers, J. A.; Frankel, R. B.; Papaefthymiou, G. C.; Holm, R. H. *J. Am. Chem. Soc.* **1977**, *99*, 84−98.
(38) Lane, R. W.; Ibers, J. A.; Frankel, R. B.; Holm, R. H. *Proc. Natl. Acad. Sci. U.S.A.* **1975**, *72*, 2868−72.
(39) Beissel, T.; Buerger, K. S.; Voigt, G.; Wieghardt, K.; Butzlaff, C.; Trautwein, A. X. *Inorg. Chem.* **1993**, *32*, 124−6.
(40) Fallon, G. D.; Gatehouse, B. M. *J. Chem. Soc., Dalton Trans* **1975**, 1344−47.
(41) Fallon, G. D.; Gatehouse, B. M.; Marini, P. J.; Murray, K. S.; West, B. O. *J. Chem. Soc., Dalton Trans* **1984**, *12*, 2733−9.
(42) Snow, M. R.; Ibers, J. A. *Inorg. Chem.* **1973**, *12*, 249−51.
(43) Shoner, S. C.; Barnhart, D.; Kovacs, J. A. *Inorg. Chem.* **1995**, *34*, 4517−18.
(44) Greenwood, N. N.; Earnshaw, A. In *Chemistry of the Elements*; Pergamon Press: New York, 1984; p 1266.
(45) Cotton, F. A.; Wilkinson, G. In *Advanced Inorganic Chemistry*; 4th ed.; Wiley: New York, 1980; pp 648−9 and 761−2.
(46) Leipoldt, J. G.; Coppens, P. *Inorg. Chem.* **1973**, *12*, 2269−2274.
(47) Schaffer, C. E.; Jorgensen, C. K. *J. Inorg. Nucl. Chem.* **1958**, *8*, 143.
(48) Shoner, S. C.; Olmstead, M. M.; Kovacs, J. A. *Inorg. Chem.* **1994**, *33*, 7−8.
(49) Shoner, S. C.; Humphreys, K.; Barnhart, D.; Kovacs J. A. *Inorg. Chem.* **1995**, *34*, 5933−34.
(50) Shoner, S. C.; Nienstedt, A.; Ellison, J. J.; Kung, I.; Barnhart, D. Kovacs, J. A. *Inorg. Chem.* **1997**, submitted.
(51) Jackson, H. L.; Shoner, S. C.; Barnhart, D.; Kovacs, J. A. Manuscript in preparation.
(52) Coucouvanis, D.; Swenson, D.; Baenziger, N. C.; Murphy, C.; Holah, D. G.; Sfarnas, N.; Simopoulos, A.; Kostikas, A. *J. Am. Chem. Soc.* **1981**, *103*, 3350−3362.
(53) Holm, R. H.; Ibers, J. A. *Iron−Sulfur Proteins*; Academic Press: New York, 1977; Vol. III, Chapter 7.
(54) Duggan, D. M.; Hendrickson, D. N. *Inorg. Chem.* **1975**, *14*, 955.
(55) Live, D. H.; Chan, S. I. *Anal. Chem.* **1970**, *42*, 791.

voltammograms were obtained using a PAR 273 potentiostat with a glassy carbon working electrode, a platinum wire counter electrode, an SCE reference electrode, and 0.1 M (n-Bu_4N)(PF_6) supporting electrolyte.

Synthesis of 3-Methyl-3-mercapto-2-butanone. Sodium hydroxide (8 g, 200 mmol) was dissolved in 100 mL of MeOH. This solution was degassed and cooled to −15 °C and then saturated with H_2S. 3-Methyl-3-chloro-2-butanone[56] (24.1 g, 200 mmol) was added dropwise to this solution over 1 h, resulting in the formation of a white precipitate (NaCl). The bath temperature was then allowed to warm in increments. First it was warmed to −5 °C stirred for 1 h, and then warmed to room temperature and stirred for an additional hour. An aqueous acidic solution (H_2O/H_2SO_4, pH = 4, 100 mL) was then added and the product was extracted with methylene chloride (4 × 25 mL). The extract was dried over $MgSO_4$ and then filtered. Methanol and methylene chloride were removed by distillation at ambient pressure. 3-Methyl-3-mercapto-2-butanone was then isolated, as a foul smelling colorless liquid, by distillation at 85 °C at reduced pressure. Yield: 18.2 g (77%). ^{1}H NMR ($CDCl_3$): δ1.48 (6, CH_3), 2.01(1, SH), 2.30 (3, CH_3). ^{13}C NMR ($CDCl_3$): δ 23.75, 27.68, 50.29, 207.38.

Synthesis of [$Fe^{III}S_2^{Me2}N_3$(Pr,Pr)]PF_6 (2). A solution of 3-methyl-3-mercapto-2-butanone (0.71 g, 6 mmol) was dissolved in 10 mL of MeOH. To this was added 1 equiv of NaOMe in 10 mL of methanol, and the mixture was stirred for 10 min. 3,3′-Iminobis(propylamine) (0.42 mL, 3 mmol) was then added to this mixture via syringe, and the resulting solution was allowed to stir for 20 min, and then cooled to −40 °C. This solution was then added dropwise to a solution of anhydrous ferrous chloride (0.38 g, 3 mmol) in 20 mL of MeOH also cooled to −40 °C. The resulting reaction mixture was allowed to stir for 3 h and then stored in a freezer overnight. The following day, 1 equiv of Cp_2FePF_6 (1 g, 3 mmol) in 10 mL of MeCN was added dropwise to the yellow brown reaction mixture to afford an intense red-brown solution. The mixture was stirred for 30 min and then placed in a freezer overnight. The volume of the solution was then reduced to 4 mL and filtered over Celite to remove precipitated ferrocene. All volatiles were then removed under vacuum and the remaining ferrocene was extracted with Et_2O (3 × 5 mL, or until no ferrocene was present in the Et_2O washings). The remaining solids were dissolved in a minimal amount of MeCN (∼4 mL), layered with 25 mL of Et_2O, and cooled at −40 °C for ∼12 h to afford 0.66 g of dark red crystalline [$Fe^{III}S_2^{Me2}N_3$(Pr,Pr)]PF_6 (**2**; 2,3,13,14-tetramethyl-4,8,12-triaza-3,12-pentadecadiene-2,14-dithiolato iron(III)). Yield: 41%. Absorption spectrum (MeOH): λ_{max} (ϵ_M) 316 (6800), 416 (4200), 474 (sh), 774 (440) nm. Ambient temperature μ_{eff} = 3.5 μ_B in MeOH solution. IR ν(cm^{-1}): 1625 (imine). Anal. Calcd for $FeC_{16}H_{31}N_3S_2PF_6$: C, 36.23; H, 5.89; N, 7.92; S, 12.09. Found: C, 35.74; H, 6.02; N, 7.80; S, 11.95. ^{1}H NMR (CD_3CN): δ 260, 245, 104, 59 (CH_3), 57 (CH_3), 35, 20, 14 (CH_3), 11 (CH_3), −18, −21, −31.

Synthesis of [$Fe^{III}S_2^{Me2}N_3$(Pr,Pr)(N_3)] (3). A solution of tetrakis-(n-butyl)ammonium azide (0.57 g, 2 mmol) in ∼1 mL of MeCN was carefully layered on top of a solution of [$Fe^{III}S_2^{Me2}N_3$(Pr,Pr)]PF_6 (**2**) (0.42 g, 0.79 mmol), also in ∼1 mL of MeCN, and the two solutions were allowed to slowly (∼24 h) diffuse together. Diethyl ether ∼2 mL was then layered onto this solution, and the reaction mixture was cooled to −40 °C overnight to afford 0.167 g of [$Fe^{III}S_2^{Me2}N_3$(Pr,Pr)-(N_3)] (**3**) as a dark yellow crystalline solid. Yield: 36%. Absorption spectrum (MeOH): λ_{max} (ϵ_M) 330 (7400), 460 (2200), 708 (1600) nm. Ambient temperature (299 K) μ_{eff} = 2.15 μ_B in MeCN solution. IR ν(cm^{-1}): 2023 (azide), 1609 (imine). Anal. Calcd for $FeC_{16}H_{31}N_6S_2$: C, 44.96; H, 7.31; N, 19.67; S, 15.00. Found: C, 44.53; H, 6.89; N, 19.25; S, 14.95.

Azide Binding Studies. Azide binding studies were performed using freshly prepared solutions of [$Fe^{III}S_2^{Me2}N_3$(Pr,Pr)]PF_6 (**2**) and NaN_3 in MeOH. Equilibrium constants were determined by monitoring electronic spectral changes at four different temperatures (−77 °C, −41 °C, −15 °C, and 0 °C). Low-temperature spectra were obtained using a custom-designed low-temperature quartz optical dewar filled with the appropriate cooling bath (acetone/CO_2 (−77 °C), acetonitrile/N_2 (−41 °C), ethlyene glycol/CO_2 (−15 °C), and ice water (0 °C)). Concentrations for all low-temperature measurements were corrected for changes in the volume of methanol upon cooling.[57] To minimize error in our measurements, electronic spectral data was collected at the wavelength (420 nm) which displays the greatest difference in absorbance for the two complexes of interest—[$Fe^{III}S_2^{Me2}N_3$(Pr,Pr)]PF_6 (**2**) vs [$Fe^{III}S_2^{Me2}N_3$(Pr,Pr)(N_3)] (**3**). Initial concentrations of [$Fe^{III}S_2^{Me2}N_3$-(Pr,Pr)]PF_6 (**2**) ([**2**]$_0$) were allowed to vary from 0.26 to 0.36 mM. Solutions were prepared by varying the ratio of [N_3^-]$_0$ to [**2**]$_0$ so that 20% to 80% of the iron complex was azide bound. This range gave the least amount of error. Extinction coefficients for the azide-bound species (ϵ_3), [$Fe^{III}S_2^{Me2}N_3$(Pr,Pr)(N_3)]PF_6 (**3**), were obtained at −77 °C using a 50−100-fold excess of azide. Complete binding under these conditions was confirmed by showing that further addition of azide had no influence on the spectrum. The 420 nm extinction coefficient of [$Fe^{III}S_2^{Me2}N_3$(Pr,Pr)]PF_6 (**2**) (ϵ_2(420 nm)) was measured at all four temperatures, and shown to vary from 4500 M^{-1} cm^{-1} at 0 °C to 5300 M^{-1} cm^{-1} at −77 °C. The 420 nm extinction coefficient for [$Fe^{III}S_2^{Me2}N_3$(Pr,Pr)(N_3)]PF_6 (**3**) (ϵ_3(420 nm)) was determined to be 1950 M^{-1} cm^{-1} at −77 °C, and for the purposes of these calculations was assumed to be invariant upon warming. Equilibrium constants were calculated using eqs 1 and 2,[58,59] and determined to be K_{eq} (−77 °C)= 1200 ± 120 M^{-1}, K_{eq} (−41 °C) = 200 ± 20 M^{-1}, K_{eq} (−15 °C) = 66 ± 7 M^{-1}, and K_{eq} (0 °C) = 23 ± 3 M^{-1}. Thermodynamic parameters, $\Delta H = -5.2 \pm 0.9$ kcal/mol and $\Delta S = -12.4 \pm 0.4$ eu, were determined from a van't Hoff plot. Solutions were maintained at constant ionic strength ([i] = 0.12 ± 0.02 M) using an appropriate mass of $NaPF_6$.

$$[\mathbf{3}] = \frac{A - \epsilon_2[\mathbf{2}]_0}{\epsilon_3 - \epsilon_2} \quad (1)$$

$$K_{eq} = \frac{[\mathbf{3}]}{([\mathbf{2}]_0 - [\mathbf{3}])([N_3^-]_0 - [\mathbf{3}])} \quad (2)$$

CO Binding to [$Fe^{II}S_2N_3$(Pr,Pr)] (4) Monitored Spectrophotometrically. A MeOH solution of $Fe^{II}S_2N_3$(Pr,Pr) (**4**), (0.0916 mM) was placed in a custom designed low-temperature quartz optical dewar filled with the appropriate cooling bath (acetone/$N_{2(l)}$ (−97 °C), $CHCl_3$/$N_{2(l)}$ (−65 °C), acetonitrile/$N_{2(l)}$ (−46 °C), ice/salt bath (−21 °C), ice bath (0 °C), and tap water equilibrated to ambient temperature (23 °C)), and capped with the appropriate sized septum. An ambient temperature measurement of $Fe^{II}S_2N_3$(Pr,Pr) (**4**) was taken prior to carbon monoxide addition. Carbon monoxide addition was carried out using a syringe needle connected to three inches of small bore (∼1 mm o.d.) polypropylene HPLC tubing, which was inserted into the reaction flask prior to CO addition so that it sat at the bottom of the cell. CO was bubbled through the solution via the syringe needle at a rate of ∼1−2 bubbles/s, and vented through a small bore exit needle. After 3 min of bubbling, the exit needle was removed, followed by the CO addition needle, so as to allow a slight positive pressure to build in the cell, so as to counteract the cooling contraction of both the methanol and the headspace above the solution. Spectra were recorded using a Hewlett-Packard Model 8450 spectrometer, interfaced to an IBM PC.

CO Binding to [$Fe^{II}S_2N_3$(Pr,Pr)] (4) Monitored by Infrared Spectroscopy. CO binding to [$Fe^{II}S_2N_3$(Pr,Pr)] (**4**) was detected by IR in both $CHCl_3$ and MeOH solutions. Approximately 200−400 mg of **4** were placed in a 50-mL anaerobic flask equipped with a stir bar, and then dissolved in 10−30 mL of distilled/degassed MeOH. This solution was then freeze−thaw degassed three times, and CO was then bubbled through the solution for ∼5 min. Once the solution was saturated with CO (g) it was frozen under a CO atmosphere. Following the collection of a background scan using a MeOH solution saturated with CO (g), the CO saturated sample of **4** was allowed to thaw and then immediately loaded, via syringe, into a solution IR cell. Spectra were collected on a Perkin-Elmer 1600 FTIR. To rule out the possibility that MeOH solvent was reacting with the CO-ligated Fe^{II} derivative,

(56) Wyman, D. P.; Kaufman, P. R. *J. Org. Chem.* **1964**, *29*, 1956.

(57) In *Lange's Handbook of Chemistry*, 12th ed.; Dean, J. A., Ed.; Mcgraw-Hill: New York, 1979; Chapter 10, pp 127−128.

(58) Guidry, R. M.; Drago, R. S. *J. Am. Chem. Soc.* **1973**, *95*, 6645.

(59) Epley, T. D.; Drago, R. S. *J. Am. Chem. Soc.* **1969**, *91*, 2883.

Table 3. Crystal Data, Intensity Collections,[a] and Structure Refinement Parameters for $[Fe^{III}S_2^{Me2}N_3(Pr,Pr)]PF_6$ (**2**) and $[Fe^{III}S_2^{Me2}N_3(Pr,Pr)(N_3)]$ (**3**)

	2	**3**
formula	$FeS_2N_3C_{16}H_{31}PF_6$	$FeS_2N_6C_{16}H_{31}$
fw	530.38	427.44
unit cell	monoclinic	monoclinic
a, Å	13.206(3)	16.094(2)
b, Å	11.913(2)	11.022(2)
c, Å	14.944(3)	11.281(2)
α, deg		
β, deg	101.70(3)	96.33(2)
γ, deg		
V, Å^3	2306.0(12)	1988.9(10)
Z	4	4
D(calc), g/cm^3	1.528	1.427
space group	$P2_1/c$	*Cc*
absorption coefficient μ, cm^{-1}	9.60[b]	9.80[b]
transmission factors	0.9514−0.9264	0.9138−0.8604
R[c]	0.043	0.028
R_w	0.057	0.038
goodness of fit	1.15	1.06

[a] In all cases: Mo Kα(α,⁻) (λ = 0.71073 Å) radiation; graphite monochromator; −90 °C. [b] A semiemperical absorption correction was applied. [c] $R = \sum ||F_o| - |F_c|| / \sum |F_o|$; $R_w = [\sum w(|F_o| - |F_c|)^2/\sum wF_o^2]^{1/2}$, where $w^{-1} = [\sigma^2_{count} + (0.05\ F^2)^2]/4F^2$.

the above experiments were repeated in $CHCl_3$, and the IR results were shown to be identical.

X-ray Crystallographic Structure Determinations. Crystals of **2** and **3** were immersed in oil inside a drybox and then a suitable crystal of each was mounted on a glass fiber with silicon grease, and immediately placed in a low-temperature N_2 (g) stream. X-ray data was collected at −90 °C using an Enraf-Nonius CAD4 diffractometer (MoKα, λ = 0.71069 Å) equipped with a low-temperature device. Calculations were carried out on a Gateway 2000 486DX2150 computer with XCAD4 SHELXPLUS (pc version) software. Scattering factors were from taken from a standard source.[60] A ψ scan absorption correction of a high χ reflection was performed for both compounds. X-ray data collection parameters are summarized in Table 3.

Large dark red rhomboids of **2** were grown from a MeOH/MeCN solution (9:1) layered with Et_2O in a −40 °C freezer. Twenty-five reflections in the range 2θ = 30−40° were found and centered to determine the cell constants and orientation matrix. Data reduction was carried out using the XCAD4 data reduction program. Standard reflections examined after every 200 reflections showed no signs of decay. The systematic absences *h*0*l* ($l = 2n + 1$) and 0*k*0 ($k = 2n + 1$) uniquely define the space group of **2** as $P2_1/c$. The structure was determined using direct methods. Hydrogen atoms were included at calculated positions and refined using a riding model. The PF_6^- counterion was found to be disordered over two positions related by a rotation about the F(1)−P−F(2) axis. Refinement of occupancy gave a 64:36 ratio for these two molecular orientations. All non-hydrogen atoms were refined anisotropically, and the final cycle of full-matrix least squares refinement gave an *R* value of 4.3% for 300 parameters with 2480 reflections with $F > 4.0\sigma(F)$.

Dark yellow cubes of **3** were obtained by cooling a concentrated MeCN solution of **2** in the presence of 4 equiv of tetrabutylammonium azide. Determination of the crystal orientation was as for **2**; data reduction was carried out using XCAD4. Standard reflections examined after every 200 reflections showed no signs of decay. Two possible space groups, *Cc* and *C*2/*c*, were suggested by the systematic absences. *Cc* was chosen and confirmed by subsequent successful refinement. The iron atom was located in a Patterson map. All remaining non-hydrogen atoms were located in subsequent least squares refinement. Hydrogen atoms were included at calculated positions, and refined using a riding model. Final full-matrix least squares refinement gave an *R* value of 2.8% for 1778 observed reflections with $F > 4.0\sigma(F)$ and 225 parameters. A complete list of bond distances and angles for **2** and **3** are contained in the Supporting Information. Selected metrical parameters for **2** and **3** and compared in Table 4. Further details are available in the Supporting Information.

(60) Cromer, D. T.; Waber, J. T. *International Tables for X-ray Crystallography*; Kynoch Press: Birmingham, England, 1974; Vol. IV.

Table 4. Comparison of Selected Metrical Parameters for Five-Coordinate Oxidized $[Fe^{III}(S_2^{Me2}N_3(Pr,Pr))]^+$ (**2**), Five-Coordinate Reduced $[Fe^{II}(S_2N_3(Pr,Pr))]$·EtOH (**4**), and Azide-Bound $[Fe^{III}(S_2^{Me4}N_3(Pr,Pr))(N_3)]$ (**3**)

	4	**2**	**3**
Fe−S(1)	2.363(1) Å	2.133(2) Å	2.196(1) Å
Fe−S(2)	2.342(1) Å	2.161(2) Å	2.209(1) Å
Fe−N(1)	2.168(3) Å	1.967(4) Å	1.978(3) Å
Fe−N(3)	2.183(4) Å	1.954(4) Å	1.970(3) Å
Fe−N(2)	2.181(3) Å	2.049(4) Å	2.157(3) Å
mean C=N imine	1.276(4) Å	1.279(9) Å	1.289(1) Å
Fe−N(4)	N/A	N/A	2.061(4) Å
N(4)−N(5)	N/A	N/A	1.189(5) Å
N(5)−N(6)	N/A	N/A	1.162(5) Å
N(1)−Fe−N(3)	167.7°	178.1(2)°	174.9(1)°
S(1)−Fe−S(2)	124.3°	121.0(1)°	95.3(1)°
S(2)−Fe−N(2)	114.0(1)°	106.5(1)°	90.6(1)°
S(1)−Fe−N(2)	121.6°	132.3(1)°	172.5(1)°
N(1)−Fe−S(1)	82.9(1)°	86.7(1)°	84.8(1)°
N(1)−Fe−S(2)	104.7(1)°	95.2(1)°	90.8(1)°
N(1)−Fe−N(2)	87.6(1)°	94.2(2)°	99.7(1)°
N(3)−Fe−S(1)	101.7(1)°	91.6(1)°	93.7(1)°
N(3)−Fe−S(2)	82.3(1)°	86.4(1)°	84.4(1)°
N(3)−Fe−N(2)	80.3(1)°	86.2(2)°	82.2(1)°
N(4)−Fe−S(2)	N/A	N/A	173.3(1)°
N(4)−Fe−N(1)	N/A	N/A	88.8(1)°
N(4)−Fe−N(2)	N/A	N/A	82.9(1)°
N(4)−Fe−S(1)	N/A	N/A	91.3(1)°
N(4)−Fe−N(3)	N/A	N/A	96.2(1)°
Fe−N(4)−N(5)	N/A	N/A	118.5(3)°
N(4)−N(5)−N(6)	N/A	N/A	179.7(5)°

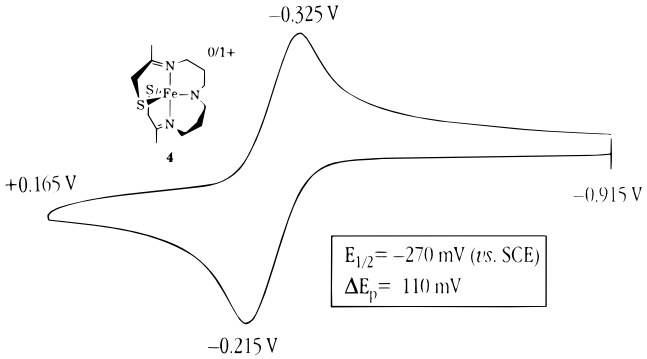

Figure 1. Cyclic voltammogram (100 mV/s) of $[Fe^{II}S_2N_3(Pr,Pr)]$ (**4**) in MeOH solution at 297 K; peak potentials vs SCE are indicated.

Results and Discussion

Synthesis of a Five-Coordinate Fe(III) Complex. In a recent paper[50] we described the synthesis and structure of the five-coordinate thiolate-ligated complex $[Fe^{II}S_2N_3(Pr,Pr)]$ (**4**), which contains high-spin Fe^{II} wrapped in a chiral helical ligand.

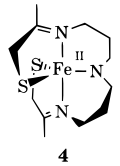

4

The discovery that the metalloenzyme NHase[1−15] contains an Fe^{III} ion in a coordination environment similar to that of **4** prompted us to examine the oxidation chemistry of **4**. As shown in the reversible cyclic voltammogram depicted in Figure 1, $[Fe^{II}S_2N_3(Pr,Pr)]$ (**4**) can be reversibly oxidized to its Fe^{III} form

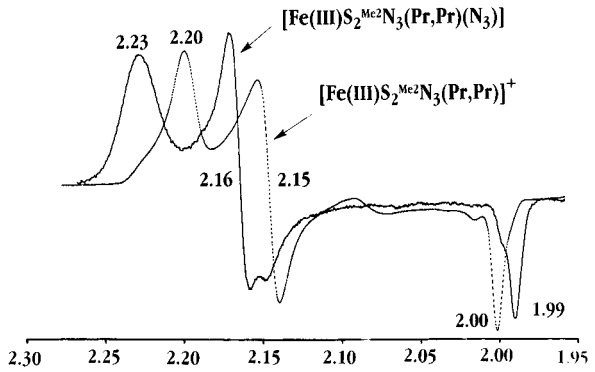

Figure 2. X-band EPR spectrum of $[Fe^{III}S_2{}^{Me2}N_3(Pr,Pr)]^+$ (**2**) vs $[Fe^{III}S_2{}^{Me2}N_3(Pr,Pr)(N_3)]$ (**3**) in MeOH/EtOH (9:1) glass at 125 K. Microwave frequency, 9.404 GHz (for **2**) and 9.214 GHz (for **3**); power, 50 mW; modulation amplitude, 1 mT; modulation frequency, 100 kHz; receiver gain, 6.3×10^4.

at a potential of −270 mV, on the electrochemical time-scale (1−200 mV/s) vs SCE. Attempts to chemically oxidize **4** using mild oxidants, failed, however, to give an isolable product. Since steric bulk has been shown to stabilize higher oxidation state metal thiolates,[34,35,61] if it is strategically placed near the ligating sulfurs, we decided to pursue this route toward our oxidized Fe^{III} derivative. If *gem*-dimethyls are incorporated into the structure of **4**, adjacent to the thiolate sulfurs, then clean oxidation of pale yellow-green $[Fe^{II}S_2{}^{Me2}N_3(Pr,Pr)]$ to its intense red/brown Fe^{III} derivative, $[Fe^{III}S_2{}^{Me2}N_3(Pr,Pr)]^+$ (**2**), is observed, with $[Cp_2Fe]PF_6$ used as an oxidant. This contrasts with the behavior of most Fe^{II} thiolates which decompose upon oxidation.[37,52]

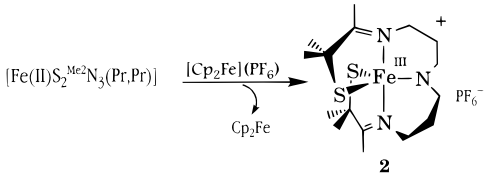

Properties of $[Fe^{III}S_2{}^{Me2}N_3(Pr,Pr)]^+$ (2). Unlike most Fe^{III} thiolate complexes, $[Fe^{III}S_2{}^{Me2}N_3(Pr,Pr)]^+$ (**2**) possesses a low-spin $S = {}^1/_2$, as opposed to a high-spin $S = {}^5/_2$, ground state. This is particularly unusual for a five-coordinate structure. Reduced $[Fe^{II}S_2N_3(Pr,Pr)]$ (**4**), on the other hand, possesses a high-spin $S = 2$ ground state. Solid-state magnetic data (Figure S1) obtained over the temperature range 4−300 K shows that the magnetic moment (μ_{eff}) of **2** is relatively constant (2.3 μ_B) between 4 and 50 K, and characteristic of an $S = {}^1/_2$ system. Between 50 and 150 K the moment gradually rises to 5.0 μ_B, and then remains constant up to 300 K, suggesting that a higher spin-state is thermally accessible. The ambient temperature solution magnetic moment of **2**, $\mu_{eff} = 3.5\ \mu_B$, is also indicative of a spin mixture at higher temperatures.[62] At, or below, 125 K, on the other hand, an $S = {}^1/_2$ state appears to be predominantly populated as demonstrated by the EPR spectrum shown in Figure 2. No signals attributable to high-spin species[63] were detected. The *g* values associated with **2** are compared with those of NHase, oxidized cytochrome P-450,[64] as well as other low-spin synthetic heme[65] and non-heme[43,51] thiolate-ligated Fe^{III} compounds in Table 1. All are characteristic of an $S = {}^1/_2$ system. The unusually small (<2.3) g_{max} values of the non-heme, thiolate-ligated iron sites suggest that the odd electron is delocalized onto the coordinated ligands in these structures.

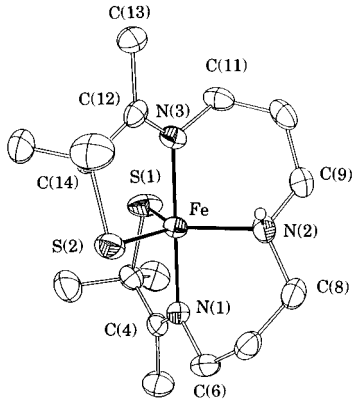

Figure 3. ORTEP plot of five-coordinate $[Fe^{III}S_2{}^{Me2}N_3(Pr,Pr)]^+$ (**2**) showing 50% probability ellipsoids and atom labeling scheme. All H atoms, except for the N(2)−H proton, have been omitted for clarity.

X-ray Structure of $[Fe^{III}S_2{}^{Me2}N_3(Pr,Pr)]^+$(2). Single crystals of the hexafluorophosphate salt of $[Fe^{III}S_2{}^{Me2}N_3(Pr,Pr)]^+$ (**2**) were grown by layering Et_2O on a MeOH/MeCN (9:1) solution. An ORTEP diagram of **2** is shown in Figure 3. Selected metrical parameters for oxidized $[Fe^{III}S_2{}^{Me2}N_3(Pr,Pr)]^+$ (**2**) are compared with corresponding parameters for reduced $[Fe^{II}S_2N_3(Pr,Pr)]$ (**4**)[50] in Table 4. Both structures have been given a consistent numbering system, so that S(2) in **2** corresponds to S(2) in **4**, etc. Structure **4** is described in detail in a separate paper.[50] Comparison of structures **2** and **4** shows that the angles about the iron change in response to metal ion oxidation, and perhaps, to a lesser extent, as a result of placing methyls next to the thiolate sulfurs. The metal ions in **2** and **4** are each located in a distorted trigonal-bipyramidal five-coordinate S_2N_3 environment. The equatorial plane contains two *cis*-thiolates sulfurs (S(1) and S(2)) and an amine nitrogen (N(2)). The axial sites are occupied by imine nitrogens (N(1) and N(3)). Two five-membered (−Fe−S−CH_2−CH=N−), and two six-membered (−Fe−N−Pr−N(H)−) rings, make up the pentadentate chelate of these structures. The two six-membered rings share a common nitrogen (N(2)−H). The N(1)−Pr−N(2)H chelate ring adopts a twisted boat conformation, while the N(3)−Pr−N(2)H chelate ring adopts a chair conformation:

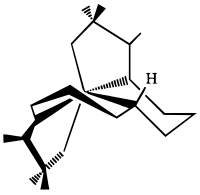

This is the usual conformational arrangement observed with structures containing two fused six-membered X−Pr−X chelate rings (X = N, O, S),[66−68] and is the only arrangement which

(61) Millar, M.; Lee, J. F.; Koch, S. A.; Fikar, R. *Inorg. Chem.* **1982**, *21*, 4105−6.

(62) Reduced **4**, on the other hand, is $S = 2$ over the entire temperature range 4−298 K. In solution, the ambient temperature magnetic moment of **4** is $\mu_{eff}(297\ K) = 5.15\ \mu_B$.

(63) Cramer, S. P.; Dawson, J. H.; Hodgson, K. O.; Hager, L. P. *J. Am. Chem. Soc.* **1978**, *100*, 7282−7289.

(64) Tsai, R.; Yu, C. A.; Gunsalus, I. C.; Peisach, J.; Blumberg, W.; Orme-Johnson, W. H.; Beinert, H. *Proc. Natl. Acad. Sci.* **1970**, *66*, 1157−1163.

(65) Tang, S. C.; Koch, S.; Papaefthymiou, G. C.; Foner, S.; Frankel, R. B.; Ibers, J. A.; Holm, R. H. *J. Am. Chem. Soc.* **1976**, *98*, 2414−2434.

(66) Zanello, P.; Cini, R.; Cinquantinin, A.; Orioli, P. *J. Chem. Soc., Dalton Trans.* **1983**, 2159.

(67) Freyberg, D. P.; Mockler, G. M.; Sinn, E. *J. Chem. Soc, Dalton Trans.* **1976**, 447.

will allow the three nitrogens involved to occupy meridional positions about the metal ion. This arrangement also places the N(2)−H proton in an axial "cyclohexyl" position so that it points away from S(1) and toward S(2). The $[S_2N_3(Pr,Pr)]^{2-}$ ligand wraps around the Fe^{III} metal ion of **2** in a helical fashion to afford a chiral molecule with $\sim C_2$ symmetry. Both enantiomers (Δ and Λ) are present in a 1:1 ratio in the crystal lattice, and related by a crystallographic inversion center. The right-handed (Δ) helical form is shown in the ORTEP diagram of Figure 3.

Comparison of Reduced $[Fe^{II}S_2N_3(Pr,Pr)]$ (4) and Oxidized $[Fe^{III}S_2{}^{Me2}N_3(Pr,Pr)]^+$ (2) Structures. As one would expect, all of the metal−ligand bond distances decrease in oxidized $[Fe^{III}S_2{}^{Me2}N_3(Pr,Pr)]^+$ (**2**) relative to reduced $[Fe^{II}S_2N_3$-(Pr,Pr)] (**4**) (Table 4). This is due, in part, to orbital contractions, but also probably reflects the change in spin state, which occur upon oxidation.[69] For example, the Fe−N distances decrease from 2.17(1) Å (imines) and 2.181(3) Å (amine) in reduced **4**, to 1.960(9) Å (imines) and 2.049(4) Å (amine) in oxidized **2**. In **2**, these distances fall at the short end of the usual range (1.93−2.01 Å (imines), and 1.97−2.21 Å (amines)) for Fe^{III} nitrogen compounds.[70,71] The mean Fe−S distance also decreases from 2.35(1) Å in reduced **4**,[50] to 2.15(2) Å in oxidized **2**. In **4**, this distance falls in the usual range for high-spin ($S = 2$) Fe^{II} thiolates. However, in **2**, this distance is noticeably shorter than most Fe^{III} thiolates[72,73] (usual range 2.18−2.30 Å). Although this may indicate that there is some sort of π interaction between the metal and sulfurs in **2**, the distorted, non-orthogonal angles in this structure (Table 4) would appear to prevent significant π overlap. The fact that the percentage decrease is approximately the same for both the Fe−S (8.8%) and Fe−N (8.3%) distances, argues in favor of something other than π interactions, as being the cause for the rather short Fe−S distances.

Influence of Spin State and Coordination Number on Bond Distances in 2. Most likely, the unusually short Fe−S distances in **2** reflect its low coordination number, coupled with its low spin-state. It is well-known that bond lengths tend to decrease as both the coordination number, and/or spin-state, of a metal complex decreases.[63] In contrast to most Fe^{III} complexes, **2** is five-coordinate, as opposed to six- or four-coordinate, and possesses an $S = {}^1/_2$, as opposed to an $S = {}^5/_2$ ground state. Since they are all $S = {}^5/_2$, even four-coordinate (lower coordination number) Fe^{III} thiolates[35,37,38,61] possess longer iron−sulfur bonds (2.25−2.30 Å) than five-coordinate **2**. Although a few six-coordinate $S = {}^1/_2$ Fe^{III} thiolates have been reported,[40,43,51] we know of no other structurally characterized five-coordinate Fe^{III}-thiolate structures possessing an $S = {}^1/_2$ ground state. Iron−sulfur distances in six-coordinate $S = {}^1/_2$ structures[40,43,51] are approximately 0.05 Å longer than those in **2**. The only other reported, structurally characterized, five-coordinate iron thiolate complexes ($[Fe^{III}N(CH_2$-*o*-$C_6H_4S)_3)$(1-Me-Im)][36] ($S = {}^5/_2$; Fe−*S* = 2.31 Å), $[Fe^{III}$(por)(S−C_6H_4−*p*-$NO_2)]$ ($S = {}^5/_2$; Fe−*S* = 2.324 Å; por = protoporphyrin IX dimethyl ester),[65] and [Fe(tsalen)(Cl)] ($S = {}^3/_2$; Fe−*S* = 2.21 Å)[41]) possess higher spin states and longer bond lengths than **2**. A similar correlation between Fe−S distances and spin state has been observed with the cysteine-ligated Fe^{III} site of cytochrome P-450.[63]

The Influence of Ligand Constraints on Bond Angles. Because the ligating atoms of $[S_2{}^{R2}N_3(Pr,Pr)]^{2-}$ are all connected in a single, fixed-length chain, constraints are placed on the allowable combinations of M−N(S) distances and N(S)−M−N(S) angles. As the metal−ligand distances change in response to changes in oxidation state and/or coordination number (vide infra), the angles about the metal ion distort so as to conform to the ligands's fixed length (Table 4). Some of the angle changes are absorbed by the Pr carbon chains, however, since bonding is more flexible to the metal, it withstands most of the distortion. The angles which are most affected by these constraints are the apical N(1)−Fe−N(3), and equatorial S−Fe−N angles. For example, as the mean Fe−N(1,3) distance decreases in going from reduced **4** to oxidized **2**, the N(1)−Fe−N(3) angle becomes more linear (Table 4). The S(2)−Fe−N(2) angle also decreases (from 114.0(1)° in **4,** to 106.5(1)° in **2**) as the apical Fe−N(1,3) separation decreases, and distorts significantly relative to the ideal 120° angle. The other angle in this equatorial plane, S(1)−Fe−N(2), opens, from 121.6 (1)° in **4** to 132.3(1)° in **2** (Table 4), in response to S(2)−Fe−N(2) closing. S(1)−Fe-S(2) remains roughly the same. The open S−Fe−N angle represents a potential binding site for small molecules, such as NHase inhibitors (N_3^-), inactivators (NO),[28,29] and possibly substrates (RCN).

Reactivity of $[Fe^{III}S_2{}^{Me2}N_3(Pr,Pr)]^+$ (2) with NHase Inhibitor N_3^-. Oxidized $[Fe^{III}S_2{}^{Me2}N_3(Pr,Pr)]^+$ (**2**) is coordinatively unsaturated with an open S(1)−Fe−N(2) angle (132.3(2)°), suggesting that the metal might be accessible to small substrates. As shown in the reaction 3, $[Fe^{III}S_2{}^{Me2}N_3(Pr,Pr)]^+$ (**2**) was found

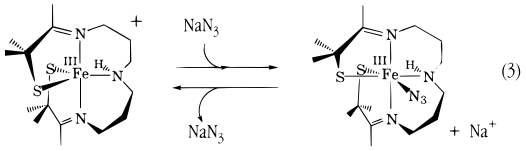

(3)

to reversibly bind azide (a NHase inhibitor) at the open S−Fe−N angle. We found no evidence for nitrile binding to **2**. Reactions between **2** and N_3^- were monitored in MeOH solution by EPR and UV/vis spectroscopy. Azide addition causes the characteristic rhombic signal associated with **2** at $g = 2.20, 2.15, 2.00$ to disappear, as illustrated in Figure 2, and be replaced by a new signal, that displays a larger g spread, and features at $g = 2.23, 2.16, 1.99$. This new signal is nearly identical to that of the azide-inhibited enzyme ($g = 2.23, 2.14, 1.99$; Table 1),[4] suggesting that (1) the iron coordination sphere in the enzyme closely resembles that of our model, and that (2) azide probably binds to the NHase iron site. If azide addition is monitored spectrophotometrically (Figure 4), then the electronic spectrum associated with five-coordinate **2** is also found to convert to one resembling NHase (Table 2). Representative results from a titration experiment, involving the addition of 0 to 80 equiv of NaN_3 to a methanolic solution of **2** at −41 °C, are shown in Figure 4. The temperature for this titration was selected so as to illustrate maximal changes in absorbance within a reasonable relative concentration range. As the azide concentration is increased the intense band at 416 (4200) nm, associated with five-coordinate **2**, decreases and two new bands

(68) Cini, R.; Orioli, P. *Inorg. Chim. Acta* **1982**, *63*, 243.

(69) In a rigorous analysis, the influence of spin-state changes on bond distances must be considered, since this would influence antibonding orbital population. However, an analysis which takes spin state into account would be complicated by the fact that **2** is mixed spin ($S = {}^1/_2/S = {}^3/_2$). A detailed molecular orbital decription along with temperature-dependent magnetic studies is therefore needed before a discussion of this type is attempted.

(70) Bernhardt, P. V.; Comba, P.; Hambly, T. W.; Lawrance, G. A. *Inorg. Chem.* **1991**, *30*, 942−946.

(71) Karlin, K. D.; Rabinowitz, H. N.; Lewis, D. L.; Lippard, S. J. *Inorg. Chem.* **1977**, *16*, 3262−3267.

(72) Marini, P. J.; Murray, K. S.; West, B. O. *J. Chem. Soc., Dalton Trans.* **1983**, 143−150.

(73) Sellmann, D.; Geck, M.; Knoch, F.; Ritter, G.; Dengler, J. *J. Am. Chem. Soc.* **1991**, *113*, 3819−3828.

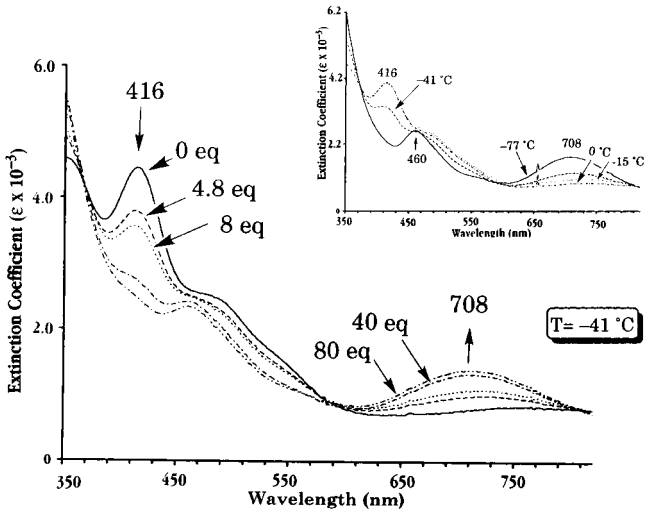

Figure 4. Titration of $[Fe^{III}S_2{}^{Me2}N_3(Pr,Pr)](PF_6)$ (**2**) (0.241 mM) with 1−80 equiv of NaN_3 in MeOH solution at −41 °C. Inset: Variable-temperature electronic spectrum of $[[Fe^{III}S_2{}^{Me2}N_3(Pr,Pr)]^+$ (**2**) (0.241 mM) + 16 equiv NaN_3 in MeOH.

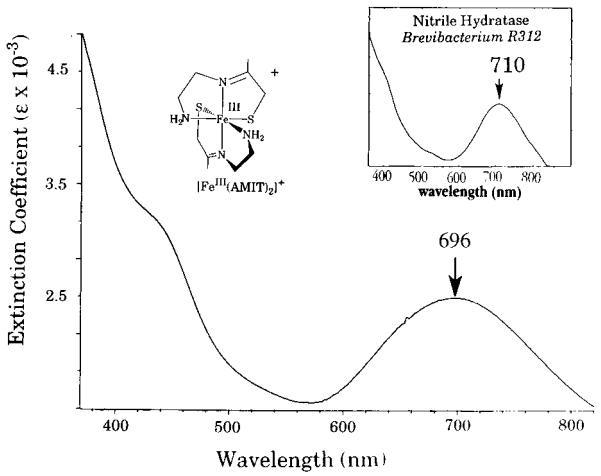

Figure 5. Electronic spectrum of $[Fe^{III}(AMIT)_2](Cl)$ (**5**) (MeCN, 298 K) vs nitrile hydratase (inset). Inset: Reprinted from ref 3. Copyright 1986 Academic Press.

at 460 (2200) nm and 708 (1600) nm grow in.[74] The low-energy band at 708 nm is characteristic of Fe^{III} in a low-spin, six-coordinate environment containing two *cis*-thiolates (Table 2). Nitrile hydratase also displays[1−4] a characteristic band in this region (Table 2), as do six-coordinate *cis*-thiolate ligated synthetic analogues $[Fe^{III}(ADIT)_2]^+$ (**1**) and $[Fe^{III}(AMIT)_2]^+$ (**5**; see Figure 5).[43] These observations suggest that azide converts five-coordinate **2** to a six-coordinate structure by binding to the iron site. In MeOH solution, complete conversion of **2** to its azide-bound form, $[Fe^{III}S_2{}^{Me2}N_3(Pr,Pr)(N_3)]$ (**3**), requires the addition of 80 equiv of N_3^- at low temperatures (−41 °C) (Figure 4). At room temperature, only small quantities of azide were found to bind, even upon the addition of up to 1000 equiv. These observations suggested that azide binds weakly to the Fe site of **2**, producing an equilibrium mixture of bound and unbound forms. The variable-temperature study shown in the inset of Figure 4 verifies that these two systems are indeed in equilibrium with one another. If a solution containing 16 equiv of azide is cooled to −77 °C, then there is a noticeable color change from orange (the color associated with **2**) to yellow-green. These changes in color were found to be reversible, and solutions were shown to revert back to their original orange color upon warming to ambient temperature, and then back, again, to their yellow-green color upon subsequent cooling. As one would expect for an associative binding process, the entropy term disfavors azide binding at higher temperatures.

(74) In MeOH, this reaction is incomplete at this temperature (−41 °C) unless 80 equiv of NaN_3 are added.

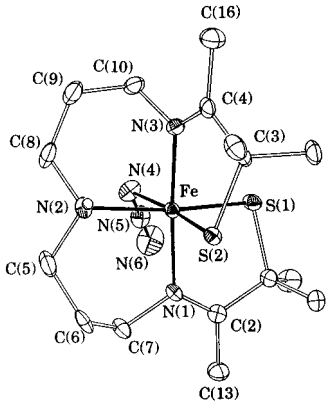

Figure 6. ORTEP plot of azide-bound $[Fe^{III}S_2{}^{Me2}N_3(Pr,Pr)(N_3)]$ (**3**) showing 40% probability ellipsoids and atom labeling scheme. All H atoms, except for the N(2)−H proton, have been omitted for clarity.

Thermodynamics of Azide Binding to 2. The reversible nature of azide binding to **2** allowed us to determine the thermodynamic parameters of binding. Equilibrium constants were determined spectrophotometrically, at constant ionic strength, using the method of Drago et al.,[58,59] at four different temperatures, and the enthalpy and entropy changes ($\Delta H = -5.2 \pm 0.9$ kcal/mol and $\Delta S = -12.4 \pm 0.4$ eu) associated with azide binding to **2** were determined from a van't Hoff plot. The rather small ΔH value supports the qualitative observations described above, and shows that azide binding to **2** is not very favorable, at least in MeOH solutions. In MeCN, on the other hand, near quantitative azide binding is observed. This dramatic influence of solvent on the equilibrium between azide-bound and azide-free **2** suggests that a favorable solvation of azide is, in part, responsible for weak azide binding to **2** in MeOH. The entropy of binding is less negative than expected for an associative process. This is most likely due to the loss of solvent ordering about neutral **3** vs ionic **2** and N_3^-.

X-ray Structure of $[Fe^{III}S_2{}^{Me2}N_3(Pr,Pr)(N_3)]$ (3). The structural features responsible for the observed weak azide binding were assessed by comparing the X-ray structures of inhibitor-free **2** and inhibitor-bound $[Fe^{III}S_2{}^{Me2}N_3(Pr,Pr)(N_3)]$ (**3**) (Figure 6)). The azide-bound form was isolated from MeCN solution, where near quantitative conversion of the azide-free to azide-bound form is observed, using only 2 equiv of $(Bu_4N)N_3$. As with **2**, both enantiomers (Δ and Λ) of **3** cocrystallize in a 1:1 ratio and are related by a crystallographic inversion center. The left-handed (Δ) helical form is shown in the ORTEP diagram of Figure 6. Selected metrical parameters for six-coordinate azide-bound $[Fe^{III}S_2{}^{Me2}N_3(Pr,Pr)(N_3)]$ (**3**) are compared with corresponding parameters for five-coordinate $[Fe^{III}S_2{}^{Me2}N_3(Pr,Pr)]^+$ (**2**) and $[Fe^{II}S_2N_3(Pr,Pr)]$ (**4**) in Table 4. All three structures have been given a consistent numbering system, so that S(2) in **3** corresponds to S(2) in **2** and **4**, etc.

Comparison of Five-Coordinate 2 and Six-Coordinate $[Fe^{III}S_2{}^{Me2}N_3(Pr,Pr)(N_3)]$ (3) Structures. The azide ligand in **3** binds trans to one of the thiolate sulfurs (S(2)) and inserts into the wider N−Fe−S angle on the side opposite to the N−H proton. The other cis sulfur (S(1)) is repelled by the azide so that the S(1)−Fe−S(2) angle closes (from 121.0(1)° in **2** to 95.3-(1)° in **3**), and S(1) is pushed toward a trans position opposite

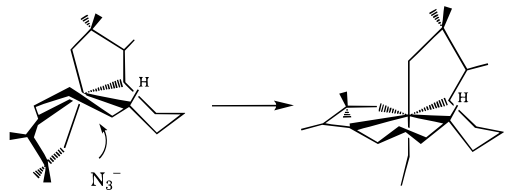

to the equatorial amine nitrogen N(2). The S(2)−Fe−N(2) angle also decreases from 106.5(1)° to 90.6(1)°. This increases the intramolecular H-bonding interaction between the amine proton and S(2); the N(2)−H···S(2) separation decreases significantly from 3.18 Å in **2** to 2.79 Å in **3**. Thus, azide binding causes the metal−ligand angles in the "equatorial" sulfur plane to convert from highly distorted trigonal (range 106.5−132.3°) in **2** to less distorted square planar (range: 82.9−95.3° (cis); 172.5−173.3° (trans)) in **3**. The $[S_2{}^{R2}N_3(Pr,Pr)]^{2-}$ ligand, on the other hand, becomes slightly more distorted as a consequence of azide binding: the angles in the N(1)−Pr−N(2) chelate ring of **3** are all significantly larger (range 113.1−113.6°) than the ideal 109.5° angle, the twisted boat chelate ring in **2** converts to a half-chair conformation in **3**, and atoms deviate more from planarity in the N(3) imine plane (±0.065 Å in **3** vs ±0.024 Å in **2**). The azide is not significantly perturbed relative to free azide or other metal-azide complexes.[75,76] An alternative binding site in this molecule would be trans to the amine nitrogen. We have not, however, observed azide binding to this site, possibly because (1) the S−M−S angle is less open, and (2) this would afford a *trans*-dithiolate. *trans*-Dithiolates are rare[77] compared to *cis*-dithiolates,[5] presumably because the trans labilizing influence of SR^- weakens the Fe−SR bonds, and thereby destabilizes the complex.

As one would expect, all of the metal−ligand bonds increase in length in response to azide binding (Table 4). For example, the mean Fe−S distance increases from 2.15(2) Å in **2** to 2.202(9) Å in **3**. This change (0.05 Å) is significantly less than the 0.2 Å change observed upon changing the oxidation state and spin state. The mean Fe−S distance in **3** falls in the range observed (2.195(6)−2.211(2) Å) with low spin ($S = {}^1/_2$), six-coordinate Fe^{III} thiolates, including $[Fe^{III}(ADIT)_2]Cl$ (**1**),[40,43,51] but is significantly shorter than that (2.28−2.32 Å) found in $S = {}^5/_2$ or $S = {}^3/_2$ Fe^{III} thiolate structures.[35−38,61,65] The mean apical imine Fe−N(1, 3) distance barely increases from 1.960(9) Å in **2** to 1.97(1) Å in **3** (Table 4). The amine Fe−N(2) distance, on the other hand, increases more noticeably from 2.049(4) Å in **2** to 2.157(3) Å in **3**. The relatively small increase in Fe imine (0.5%) vs Fe amine (5.3%) nitrogen distances may reflect the onset of π-bonding with the imine π^* orbitals in **3**. Consistent with this possibility, the $\nu_{C=N}$ IR stretch decreases from 1627 cm^{-1} in five-coordinate **2**, to 1609 cm^{-1} in six-coordinate **3**, and the mean imine C=N distance increases, slightly, from 1.28(1) Å in **2** to 1.29(1) Å in **3**. The smaller increase in Fe−S (2.3%) vs Fe−N(amine) (5.3%) distance in five-coordinate **2** vs **3**, may also reflect the onset of π bonding in **3**.

Magnetic Properties of $[Fe^{III}S_2{}^{Me2}N_3(Pr,Pr)(N_3)]$ (3). Azide-ligated **3** displays a magnetic moment of $\mu_{eff} = 2.15\ \mu_B$ in MeCN solution, consistent with an $S = {}^1/_2$ spin-state, at ambient temperature (299 K), and is $S = {}^1/_2$ over the temperature range 4−300 K in the solid state (Figure S-5). This contrasts with the magnetic behavior of **2**, and indicates that azide binding induces a greater splitting between the doublet ground state, and higher spin state(s).

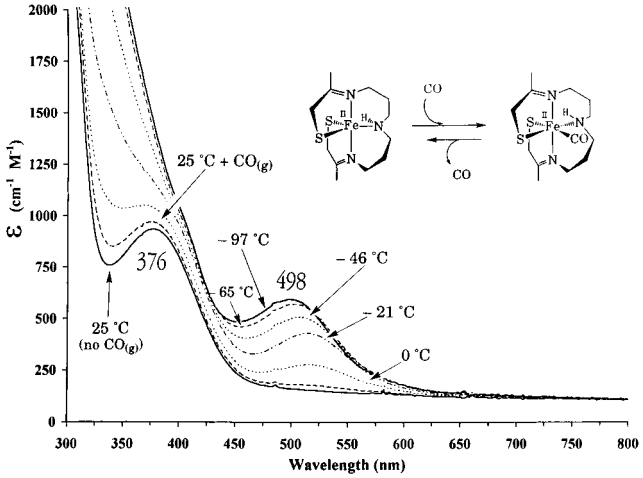

Figure 7. Variable-temperature electronic spectrum of $[Fe^{II}S_2N_3(Pr,Pr)]$ (**4**) (0.0916 m*M*) + excess CO in MeOH.

Reactivity of $[Fe^{II}S_2N_3(Pr,Pr)]$ (4) with CO. Reactivity is, in most cases, oxidation state dependent, and not surprisingly, this was found to be the case with $[Fe^{II}S_2N_3(Pr,Pr)]$ (**4**) vs $[Fe^{III}S_2{}^{Me2}N_3(Pr,Pr)]^+$ (**2**). Carbon monoxide was found to bind reversibly to reduced **4** (eq 4), but not to its oxidized Fe^{III} derivative **2**. Azide, on the other hand, was not found to bind

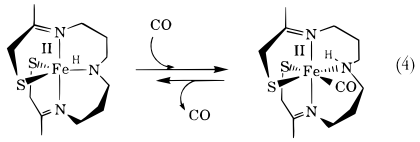

(4)

to reduced **4**. The CO-bound derivative of **4**, proposed to be $[Fe^{II}(S_2N_3(Pr,Pr))(CO)]$ (**6**), is extremely unstable, making it difficult to isolate as a solid. The variable-temperature electronic spectra shown in Figure 7, demonstrates that detectable quantities of CO-bound **6** do not form unless the temperature is decreased to near, or below, 0 °C. At ambient temperature, the spectrum is dominated by the 376-nm band associated with **4**. As the solution is cooled a new band grows in at 498 nm. The color change which occurs as a result of cooling (chartreuse green to red) is reversible, and intense red solutions formed at −97 °C convert back to their original chartreuse color upon warming, and back again to red upon cooling. The formulation of this red species as an iron-bound CO species is supported by changes which occur in the ν_{CO} region of the IR (Figure 8). MeOH, or CH_2Cl_2, solutions of **4** which have been saturated with CO (g) at −65 °C display an intense band at 1929 cm^{-1}, characteristic of an M−CO species. The relative intensities of the ν_{CO} vs $\nu_{C=N}$ bands indicate that significant, rather than trace, quantities of this species are generated. Reversible CO binding is not unusual, and is frequently observed with Fe^{II} complexes, especially in the absence of stabilizing supporting ligands. For example, $[Fe([15]aneN_4)(MeCN)(CO)]^{2+}$ ($\nu_{CO} = 1985\ cm^{-1}$),[78] is stable only at low temperatures, and readily dissociates CO as the temperature is raised. The ν_{CO} stretch of **6** suggests that there is significant π back-donation to the CO ligand, perhaps reflecting the electron donating properties of the thiolate ligands. If CO coordinates to the iron center of **4** at the site to which azide binds in **2**, then the CO would lie trans to a thiolate. Consistent with this, the CO stretching frequency associated

(75) Dori, Z.; Ziolo, R. F. *Chem. Rev.* **1973**, *73*, 247−254.
(76) Muller, A. *Struct. Bond.* **1973**, *14*, 141−171.
(77) Aruffo, A. A.; Santarsiero, B. D.; Shomaker, V.; Lingafelter, E. C. *Acta Crystallogr., Sect C* **1984**, *40*, 1693−1695.
(78) Stynes, D. V.; Hui, Y. S.; Chew, V. *Inorg. Chem.* **1982**, *21*, 1222−1225.

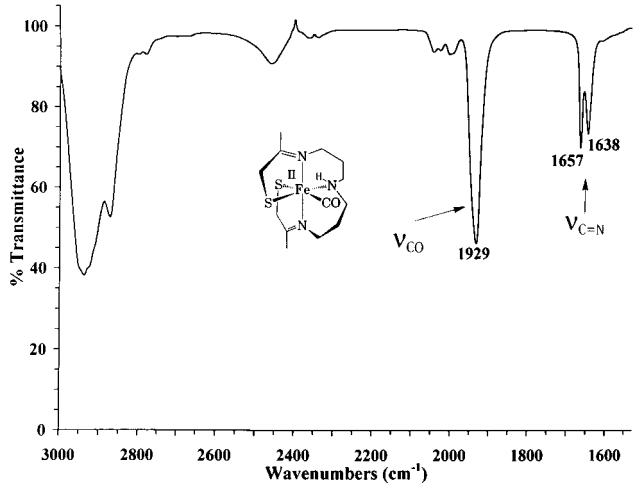

Figure 8. Solution (MeOH) IR spectrum of $[Fe^{II}S_2N_3(Pr,Pr)]$ (**4**) + excess CO.

with proposed **6** falls near, but is noticeably lower in energy (by 11−40 cm^{-1}) than, other Fe^{II} thiolate complexes containing CO trans to either O or N donors, including $[Fe^{II}(tsalen)(CO)(py)]$ (ν_{CO} = 1969 cm^{-1}; tsalen = thiosalicyclideneimine),[72] $[Fe^{II}(OS_4)(CO)]$ (ν_{CO} = 1940 cm^{-1}; OS_4= bis(2-((2-mercaptophenyl)thio)ethyl) ether),[79] and $[Fe^{II}(N_HS_4)(CO)]$ (ν_{CO} = 1950 cm^{-1}; N_HS_4= bis(2-((2-mercaptophenyl)thio)ethyl)amine).[74]

Summary and Conclusions. To summarize, a five-coordinate Fe^{III} thiolate complex $[Fe^{III}S_2{}^{Me2}N_3(Pr,Pr)]^+$ (**2**) was described which reacts with azide to form a model for the azide-inhibited form of the metalloenzyme nitrile hydratase (NHase). Steric bulk placed adjacent to the sulfurs increased the stability of **2** relative to its less sterically protected analogue. In contrast to most five-coordinate Fe^{III} complexes, **2** was shown to possess an $S = {}^1/_2$ ground state. The low spin state of **2**, coupled with its low coordination number, result in unusually short Fe−S bonds (2.15(2) Å). Ligand constraints were shown, by X-ray crystallography, to distort the S−Fe−N bond angles and thereby create an open (132.3(1)°) reactive site. There was no evidence for nitrile binding to **2**. Azide was found to bind reversibly to this site in MeOH, but irreversibly in MeCN. This demonstrates that the secondary coordination sphere (i.e., the solvent, or possibly a protein binding pocket) can have a dramatic influence on the substrate binding properties of a metal complex. Although very little has been reported about azide binding to NHase (pH dependence, etc.),[4] it is worth noting that the NHase active iron site pocket contains a mixture of hydrophobic and H-bonding residues (Ser X 2, Tyr X 4, Arg X 3, Gln X 1),[24] the latter of which perhaps modify the azide binding properties of the enzyme active site making it more accessible to nitriles. A variable-temperature equilibrium study in MeOH afforded thermodynamic parameters of binding ($\Delta H = -5.2 \pm 0.9$ kcal/mol and $\Delta S = -12.4 \pm 0.4$ eu) for this inhibitor to **2**. The nearly identical EPR parameters of $[Fe^{III}S_2{}^{Me2}N_3(Pr,Pr)(N_3)]$ (**3**) vs those for azide-inhibited NHase suggest that (1) the NHase iron coordination sphere closely resembles that of our model, and (2) azide probably binds to the NHase iron site. Prior to our work, evidence to support this was lacking. Inhibitor-bound **3** displays an intense low energy band near 700 nm, similar to the pH = 7.3 form of NHase, and other six-coordinate Fe^{III} *cis*-dithiolate complexes. Reactivity was found to be oxidation state dependent, and reduced $[Fe^{II}S_2N_3(Pr,Pr)]$ (**4**) was found to reversibly bind CO, but not azide. Oxidized **2**, on the other hand, was not found to bind CO.

Acknowledgment. We thank Henry Jackson and Dirk Schweitzer for helpful discussion, Colin Mailer for assistance with the EPR work, Vincent Huyhn for helpful discussions about the EPR work, and Alice Pereira and Pedro Tevares for reexamining the EPR properties of **2** at higher T. Financial support from the National Institutes of Health (Grant GM 45881), and the National Institute of Environmental Health Sciences (P30 ES07033; EPR spectrometer) is also gratefully acknowledged.

Supporting Information Available: Additional tables include: crystallographic data, atomic positional and thermal parameters, bond distances and angles, and calculated hydrogen atom positional parameters, for **2**, and **3**. Supplementary figures include magnetic moment (μ_{eff}(BM)) vs temperature plots for $[Fe^{III}S_2{}^{Me2}N_3(Pr,Pr)](PF_6)$ (**2**) and $[Fe^{III}S_2{}^{Me2}N_3(Pr,Pr)(N_3)]$ (**3**) (19 pages, print/PDF). See any current masthead page for ordering information and Web access instructions.

JA973129Q

(79) Sellmann, D.; Kuntsmann, H.; Knoch, F.; Moll, M. *Inorg. Chem.* **1988**, *27*, 4183−90.